27 Atomic Structure

L.J. Curtis[1] and I. Martinson[2]

[1] Department of Physics and Astronomy, University of Toledo, Toledo, Ohio 43606-3390, USA
ljc@physics.utoledo.edu
[2] Atomic Spectroscopy, Department of Physics, Lund University, Box 118, 22100 Lund, Sweden
Indrek.Martinson@fysik.lu.se

27.1 Introduction

The fact that particle accelerators can produce isotopically pure, monoenergetic beams of atomic ions over a wide range of speeds and ionic states means that these machines can be utilized to study both atomic and nuclear properties with no experimental modifications other than beam targeting and detection equipment. By a suitable choice of accelerator energy and ion source capabilities, virtually any energy level of any charge state of any atom can be studied. The excitation can be produced by impinging the beam on a thin foil, a gas cell, or either a crossed or a collinear laser beam. The deexcitation can be interrogated by microwave, optical, or x-ray detection, or by electron spectroscopy, with the possibility of time-of-flight temporal resolution.

One of the most flexible and widely used techniques is that of beam–foil spectroscopy (BFS), in which the accelerated particles impact a thin foil, within which they undergo excitation and ionization in a dense environment, and then suddenly emerge into a low-density, field-free environment. The excitation mechanism has the possibility of providing both time resolution and coherent anisotropic excitation. BFS is now a mature field (having been pursued for about 40 years), and has provided much new data, elucidated fundamental atomic processes, and furthered applications in a variety of related fields. Improved technical capabilities have now broadened its applicability to permit new types of measurements of unprecedented accuracy and scope. The experimental groups in North America and Europe that pioneered the field have now been joined by a new generation of international practitioners, with new and active groups in China, India, Japan, and South Africa, for example.

In this chapter, we shall review some of the successful applications of accelerator-based methods (giving primary emphasis to BFS), and indicate other areas that hold promise for future measurements.

27.2 The Present Status of Atomic-Structure Research

The knowledge of energy levels, transition probabilities, and other atomic-structure data has been greatly advanced by the development of new light sources and technical improvements in the use of traditional light sources, motivated by urgent applicational needs. These light sources include the use of fast ion beams, tokamak- and laser-produced plasmas, orbiting observation of astrophysical objects, recoil ions from ion–atom collisions, electron beam ion sources (EBISs) and ion traps (EBITs), electron cyclotron resonance (ECR) ion sources, ion storage rings, and Fourier transform spectroscopy (FTS), as well as improved use of traditional spark and vacuum arc sources. Since the interpretation of time-resolved measurements requires a thorough knowledge of the radiatively coupled energy-level structure, these studies must be accompanied by high-resolution wavelength and energy-level measurements.

The application of these techniques has produced large blocks of generic data, for example along isoelectronic sequences, in highly excited Rydberg series, in core-excited "hollow-atom" states, and in coherently excited "entangled" states. However, much remains to be done, particularly in the determination of relative intensities of decays from levels that have multiple exit channels (branching-fraction data) in atoms and ions.

27.3 Capabilities and Limitations of the BFS Method

The BFS light source possesses many unique characteristics that permit types of measurements that are not accessible to other methods of excitation. As is often the case, capabilities can also impose restrictions, but many features that were earlier considered as limitations have now been reduced or eliminated. A typical BFS experimental setup is shown in Fig. 27.1.

The primary advantage of BFS is its universal applicability since, given a suitable accelerator and ion source, virtually any ion of any atom can be studied in a time-resolved manner. However, because the time resolution is achieved by time-of-flight methods, this does impose limitations on the minimum and maximum time windows (ranging from the shortest beam length that can be optically resolved to the longest flight path that can be efficiently monitored). Thus the lifetime range for BFS methods is approximately 0.1 ps to 300 ns. Lifetime measurements are usually obtained by translating the foil upstream and downstream stepwise while the optics views a fixed point along the beam. This provides precise time resolution, but it also requires data collection in a multiscaling mode, with the detection apparatus sensitive to only one increment of time-since-excitation at a time. The solid foil provides a region of very high density that causes heavy excitation of all levels, including extensive core excitations. This does, however, involve nonselective excitation, so that decay curves are sums of the many exponentials that are inherent in the repopulation by cascade transitions. The density of the beam

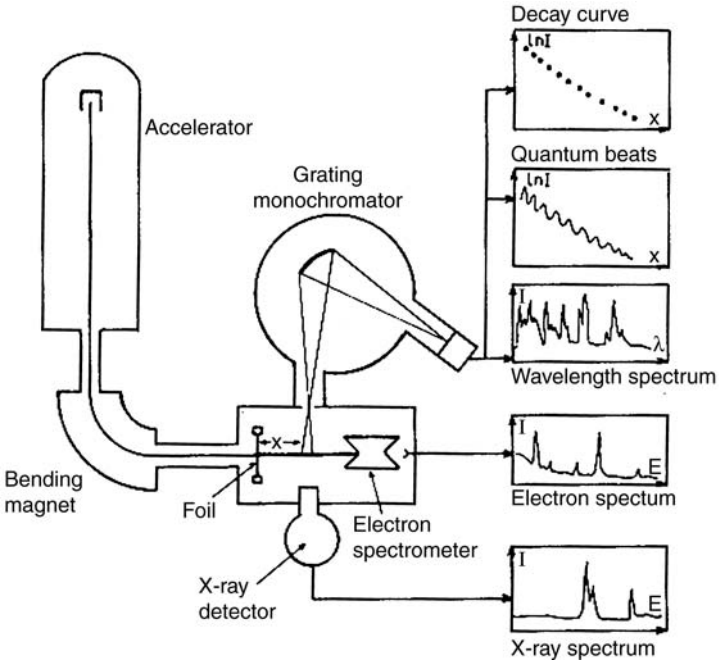

Fig. 27.1. Schematic representation of experimental arrangements for a variety of types of BFS measurements

is very low (much rarer than the residual gas even at ultrahigh vacuum), so there is no significant collisional radiation damping, and there are no significant interionic fields. Because the beam suddenly emerges from the dense foil into the evacuated flight path, the excitation can be coherent, and can exhibit interference and quantum beats. The preferred direction and the possibility of tilting the foil relative to the beam can produce useful excitation anisotropies.

A typical BFS spectrum is shown in Fig. 27.2. Here 24 MeV Fe ions from a tandem accelerator were excited in a carbon foil. The spectrum shows transitions in highly charged Fe only. Several of these lines appear in the spectrum of the solar corona and flares. However, there they are often blended with lines from other elements, for example O, S, and Cl.

27.4 Technical Developments That Enhance Capabilities

The lifetimes of excited states in atoms and ions are of interest for atomic theory, being sensitive indicators of the accuracy of the wave functions applied in calculations. Furthermore, they are also crucial for astrophysics, for example in the determination of element abundances in the Sun and stars.

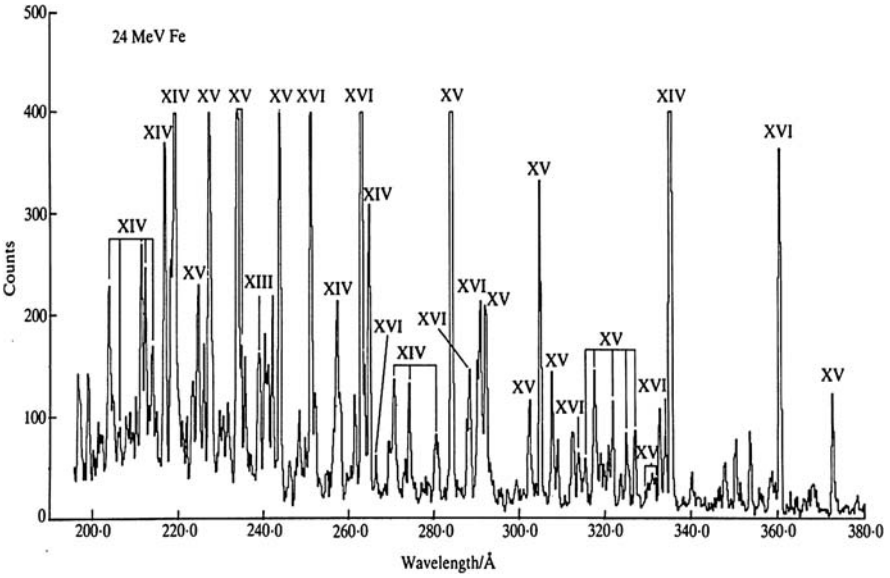

Fig. 27.2. Beam–foil spectrum of iron in the wavelength region 20–38 nm

There exist many techniques which allow such studies in neutral and singly ionized atoms, whereas BFS is the only method for highly charged ions. However, since many levels in an ion can be populated in BFS excitation, the decay curve of a given level is often complicated because of feeding from higher-lying states. In the early days of BFS, when such decay curves were analyzed by multiexponential fitting, large uncertainties (up to 50%) could be encountered. Fortunately, such problems have now been largely eliminated.

27.4.1 Elimination of Cascade Effects

The decay curve distortions introduced by cascade repopulation can be accounted for by a technique that involves measurement, under similar conditions, of the decay curve of the primary transition as well as those of all of its significant cascade feeders. This is known as the method of "adjusted normalization of decay curves"(ANDC).

The instantaneous population change of a given level is governed by the difference in transition rates between the cascades into and the decays out of that level. To within constant factors of the transition probabilities and detection efficiencies, the time dependence of these populations is specified by the variation of the detected intensities along the time-resolved decay curves. Thus, rather than expanding a single decay curve measurement on a set of mathematical exponentials, it is possible to expand the decay curve of the primary level on the measured decay curves of the cascades that repopulate

it. In this formulation, the lifetime and the detection efficiencies can be accurately extracted as linear fitting parameters, with internal-consistency criteria that test and verify whether all significant cascades have been included.

A schematic representation of an ANDC determination of the lifetime of the 6p $^2P_{3/2}$ level in Tl III is shown in Fig. 27.3. The population rate equation for this system, reexpressed in terms of measured decay curve intensities, is given by

$$\tau_{6p}\frac{dI_{6p}}{dt}(t_i) = \xi_{6d}I_{6d}(t_i) + \xi_{7p}I_{7p}(t_i) - I_{6p}(t_i)\ . \tag{27.1}$$

Here the lifetime τ_{6p} of the 6p level and the normalizations ξ_{6d} and ξ_{7s} for the 6d and 7s cascades (relative to that of the primary decay curve) are determined by simultaneous solution of the relationships provided by evaluating (27.1) at each common point t_i on the various decay curves. This method has been used to obtain many lifetimes of high reliability and precision.

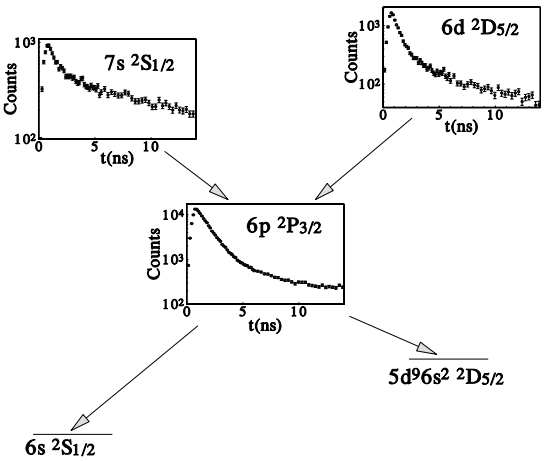

Fig. 27.3. ANDC analysis of cascade-correlated decay curves

The precise determination of this lifetime in Tl III is of application in astrophysics, because the corresponding spectral lines are observed in the spectra of so-called chemically peculiar stars. This ANDC measurement yielded a value 1.06 ± 0.04 ns (4%), as compared with earlier curve-fitted measurements, which had uncertainties of 10–20%.

27.4.2 Multiplexed Detection

Although the low particle density characteristic of BFS has many positive aspects, it also results in low intensities in the emitted light. This is exacerbated by the fact that the time-of-flight method involves single-channel detection, in

which each individual time-since-excitation is separately measured in a multiscaling mode. Thus the count rates for a specific wavelength measured at a specific time-since-excitation can be low, especially on the long-time tails of the decay curve. However, these limitations have been greatly reduced by the development of position-sensitive detectors (PSDs). While detection is still single-channel in the time domain, it is now possible to utilize multiplexed detection in wavelength. By simultaneously measuring a broad range of wavelengths at each time-since-excitation, significant advantages are achieved. A landscape plot showing a multiplexed data set (intensity vs. both wavelength and decay time) is presented in Fig. 27.4.

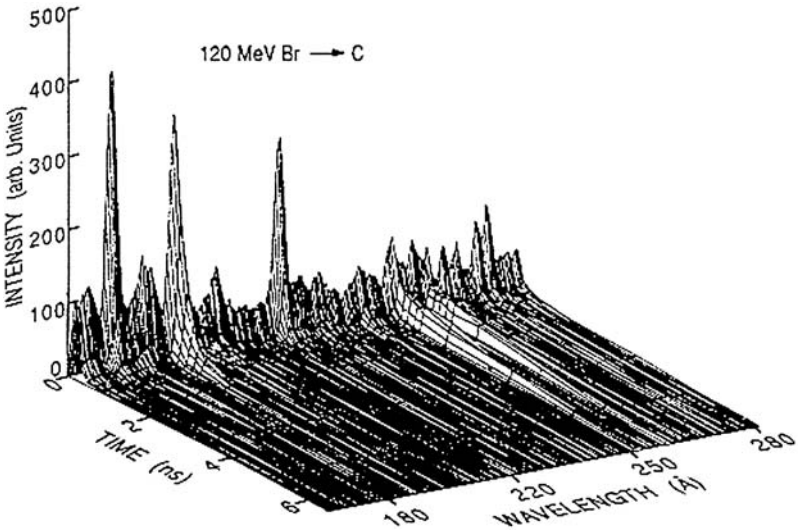

Fig. 27.4. Multiplexed landscape of intensity, wavelength, and decay time

In addition to the obvious gain in data collection efficiency afforded by a sensitivity to a broad range of wavelengths, many other advantages can be cited. By virtue of simultaneous measurement, many possible systematic uncertainties are eliminated by considering subtracted differences between the decay curves. It is also possible to examine the exponential content across a line profile to check for line blending. For systems for which the wavelengths of the primary and cascade transitions lie within the multiplexed wavelength range, it is possible to perform ANDC analyses in real time.

A significant advantage involves differential lifetime measurements, which can reveal small differences in lifetimes among the fine-structure transitions within a multiplet. Consider, for example, the fine structure of the Be-like $2s3s\ ^3S_1$–$2s3p\ ^3P_J$ transitions. Here the $J = 1$ level possesses a strong intercombination relativistic-E1 decay channel to the $2s^2\ ^1S_0$ ground state that is

forbidden to the $J = 0$ and 2 levels by angular-momentum conservation. In contrast to the usual situation, in which decay curve measurements determine only lifetimes and not branched transition probabilities, the branching fraction for this ground-state channel can be specified by differential lifetime measurements. A plot of the decay curves for these three levels in Be-like Ne VIII is shown in Fig. 27.5. In addition to their theoretical interest, such intercombination lines are also important for the diagnostics of laboratory and astrophysical plasmas.

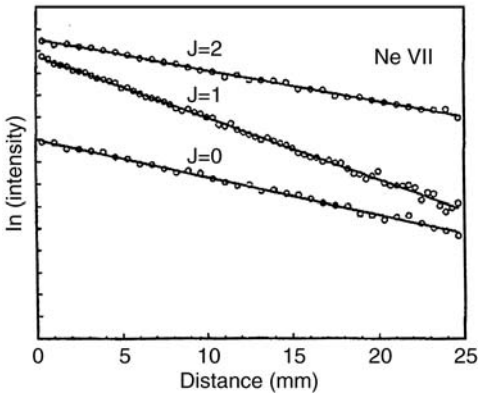

Fig. 27.5. Decay curve measurements within a fine-structure multiplet

Prior to the availability of PSD devices, these decay curves were measured separately and subtracted channel-by-channel. When the emitted radiation from all three of these transitions is detected simultaneously at each distance downstream, many systematic uncertainties cancel in differential measurements, and the precision can be greatly enhanced over previous determinations.

In this example, an extra channel to the ground state is determined by differential lifetime measurements. As will be discussed in Sect. 27.5.4, multiply excited ions sometimes possess a J-dependent autoionization channel that can be determined by using these same differential lifetime measurement methods.

Figure 27.6 shows a measurement of the quantum beats that arise from coherent excitation of fine-structure levels in He I. These frequencies represent fine-structure intervals in atoms and ions, i.e. quantities that are crucial for understanding various relativistic and higher-order effects. The relative frequency measurements in Fig. 27.6 were made with a common time base by using two different spectrometers so as to obtain a precise relative normalization. Similar measurements can now be made through PSD detection, and could provide precise accurate relative values for fine- and hyperfine-structure splittings.

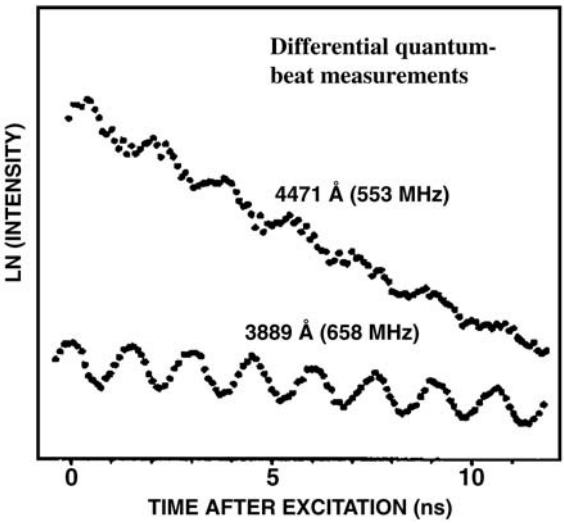

Fig. 27.6. Simultaneously measured quantum beat frequencies in He

27.5 Contributions of Accelerator-Based Studies

The use of accelerator-based measurements has produced large databases that permit comprehensive predictive, semiempirical systematizations.

27.5.1 Isoelectronic Measurements for Alkali-Metal-Like Systems

One particularly valuable application of BFS has been the study of lifetimes along isoelectronic sequences. By utilizing a variety of accelerators to trace a sequence of ions with a fixed number of electrons as a function of nuclear charge Z, it is possible to examine and separate processes that scale differently with Z. For highly charged ions, properties are often different from those observed for neutral and few-times-ionized systems (e.g., magnetic fine structure can exceed electrostatic gross structure, forbidden transitions can exceed allowed transitions, etc.). Rather than studying the lifetimes directly, these quantities can be used converted to line strength factors S_{ik}, defined theoretically in terms of the theoretical dipole transition matrix element as

$$S_{ik} = \sum_{m_i} \sum_{m_k} |\langle i|\mathbf{r}/a_0|k\rangle|^2 \ . \tag{27.2}$$

The isoelectronic behavior of S_{ik} is much more regular and slowly varying than that of the lifetime, since the latter contains sums over wavelength factors that vary rapidly as a function of nuclear charge. The line strength factor

can be deduced from the measured lifetime τ_i, the measured transition wavelength λ_{ik}, the statistical weight of the level g_i, and the branching fraction B_{ik} (unity for a decay with only one exit channel) using

$$S_{ik} = [\lambda_{ik}(\mathrm{nm})/126.538]^3 g_i B_{ik}/\tau_i(\mathrm{ns}) \ . \tag{27.3}$$

This predictive power of these isoelectronic studies is illustrated by Fig. 27.7, which shows a plot of the scaled line strength factors for the lowest resonance transitions of the Na isoelectronic sequence.

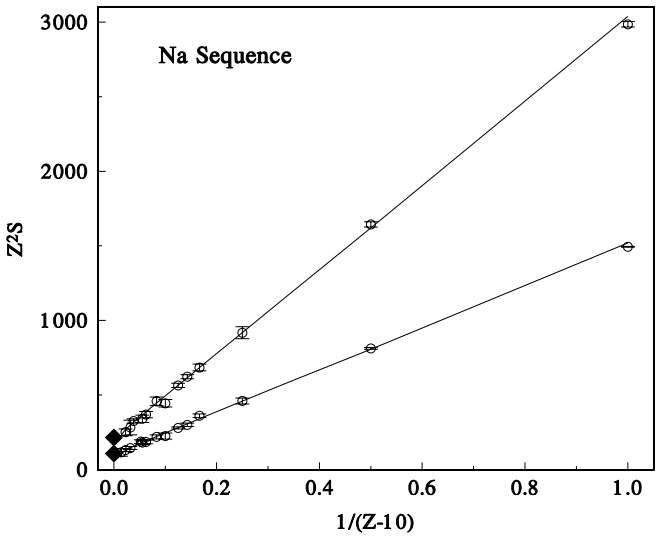

Fig. 27.7. Scaled line strengths for the 3s–3p transitions in the Na isoelectronic sequence

It has been observed that these quantities exhibit a nearly linear behavior when plotted vs. a suitably chosen reciprocal screened charge, and can be characterized by a fit to the empirical function

$$Z^2 S \approx S_{\mathrm{H}} + b/(Z - C) \ . \tag{27.4}$$

Moreover, this linearity appears to extrapolate to the hydrogenic limit at infinite Z, which is given by

$$S_{\mathrm{H}} \to 3n^2(n^2 - 1)g_i/4 \ . \tag{27.5}$$

While the extreme limit of infinite Z is clearly a nonphysical asymptote, tests have been made which indicate that this linearization remains valid through the stable isotopes.

Because of the availability of very high-energy accelerators, BFS measurements for the Li isoelectronic sequence have been extended to very high Z

and include a lifetime determination in three-electron uranium. When this result was put on a plot of the charge-scaled line strength factor, it initially appeared that there was a breakdown in this linear trend, but a subsequent analysis provided an interesting test of relativistic effects. This is shown in Fig. 27.8(a), which reveals a clear dip in value below the linear trend.

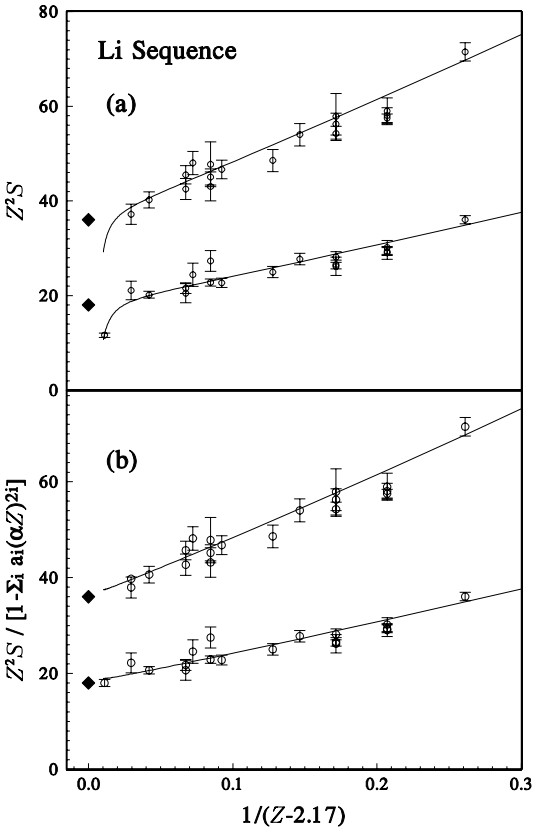

Fig. 27.8. Scaled line strengths for the Li isoelectronic sequence: (**a**) with no relativistic corrections; (**b**) with single-particle Dirac relativistic corrections

Two alternative mechanisms were considered to explain the origin of this dip. One possibility is that a many-electron redistribution of the electrons in the complex core could be occurring. A second possibility is that relativistic corrections only to the single-electron formulation of the line strength factor are occurring, with no major modification of the core. It was possible to examine these two models semiempirically. Higher-order calculations were made using the Dirac equation rather than the Schrödinger equation, and used to correct the abscissae of the measured data points for a modified

empirical fitting function given by

$$Z^2 S \left[1 - \sum_i a_i [\alpha(Z-C)]^{2i}\right]^{-1} \approx S_{\rm H} + b/(Z-C) \ . \tag{27.6}$$

As shown in Fig. 27.8(b), this second model successfully restored the linearity. Subsequent theoretical calculations have confirmed this result. Because of this linearity, it is now possible to interpolate, extrapolate, and smooth data throughout entire isoelectronic sequences. This can be done on the basis of only a few accurate measurements, sufficient to specify the empirical screening parameter C on the abscissa.

Cancellation Effects

While sufficient numbers of precision measurements now exist to permit accurate semiempirical specification of the lifetimes of the lowest resonance transitions in all alkali-metal-like systems, other transitions in these systems still pose challenges for future measurements. Transition rates among the excited states in alkali-metal-like systems are difficult to specify either experimentally or theoretically. Experimentally, the decay of each upper level is branched to many lower levels, and lifetimes cannot be converted to transition probabilities because of the lack of branching-fraction data. Theoretically, the dipole matrix elements can be affected by strong and highly localized cancellation effects that are extremely sensitive to subtle perturbations not normally accounted for in the basis set wave functions.

The sensitivity of these cancellation effects can be illustrated by the semiempirical quantum defect method, in which the term energy T for an alkali-metal-like ion can be expressed in terms of the Rydberg formula

$$T = Ry\, \zeta^2/(n^*)^2 \ . \tag{27.7}$$

Here Ry is the Rydberg constant, ζ is the net charge of the nucleus and inner core electrons, and n^* is the effective quantum number of a hydrogenlike ion that would have the same energy as the complex ion in question. Theoretical insight can be gained by writing the effective quantum number as $n^* \equiv n - \delta$, where n is the principal quantum number in a hydrogenlike atom, and the quantity δ is known as the effective "quantum defect". It can be shown that the quantum defect can be related to a phase shift in the radial wave function, whereby the radial coordinate at large r for the wave function of the complex ion is shifted by $\delta\pi$ from a corresponding hydrogenlike wave function. In the isoelectronic variation of a given transition between two excited levels, differential isoelectronic variations in the quantum defects of the upper and lower levels lead to regular cancellations in the dipole matrix element. This is illustrated Fig. 27.9, which is a plot of $n_{\rm s}^*$ vs. $n_{\rm p}^*$ for the s–p transitions in the Na isoelectronic sequence. The solid lines correspond to the nodes where

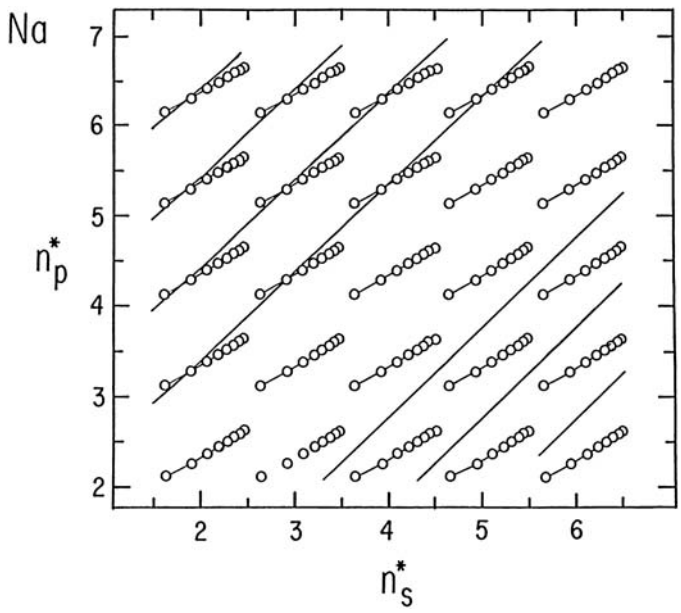

Fig. 27.9. Cancellation plot for the ns–n'p transitions in the Na isoelectronic sequence

these cancellations would be expected to occur, and the connected circles represent the experimental effective quantum numbers.

Wherever the circles fall near a nodal line, an anomalously small transition probability is expected to occur. This exposition clearly illustrates how theory can be hindered by the many cancellations that occur in these transition integrals.

Moreover, experimental measurements of line strength factors between excited levels are almost entirely lacking. These levels undergo branched decay, and lifetimes cannot be reduced to line strength factors without accompanying branching-fraction data. Because of difficulties with relative in-beam intensity calibrations, branching-fraction data for multiply charged ions are virtually nonexistent. However, new methods offer promise in this area, which will be discussed in Sect. 27.6.1.

27.5.2 Isoelectronic Measurements for Alkaline-Earth-Like Systems

These semiempirical methods can also be applied to two-valence-electron atoms. Because of the singlet–triplet nature of transitions of the form ns^2–nsnp, the resonance and intercombination transitions to ground can be related to each other through intermediate-coupling (IC) amplitudes describing the deviation of their angular-momentum states from pure LS coupling. The

IC amplitudes can be specified as mixing angles deduced from spectroscopic energy-level data.

As shown for the 5s5p transitions in the Cd sequence in the upper panel of Fig. 27.10, the singlet–triplet mixing angles can be presented on a linearized plot that converges to the jj coupling limit at infinite Z.

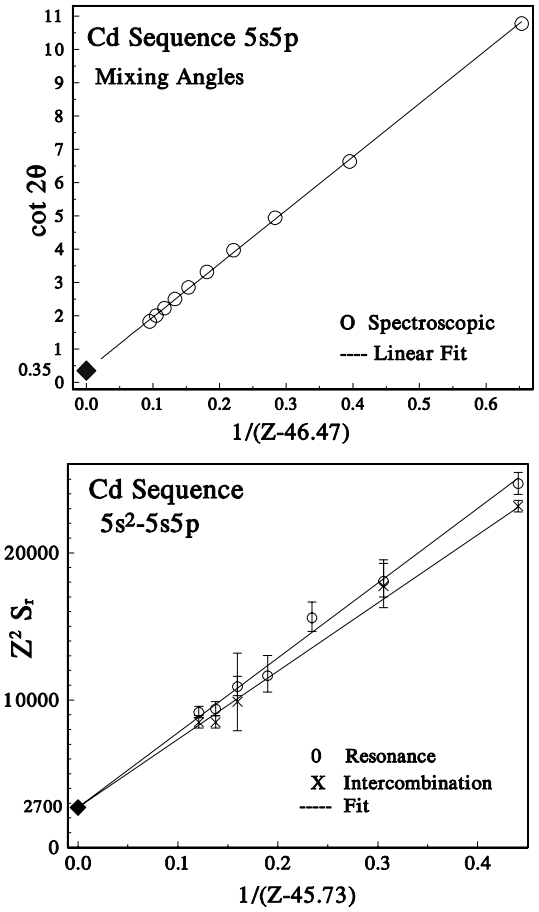

Fig. 27.10. Mixing angle and scaled reduced line strength factors for the Cd isoelectronic sequence

These mixing angles can be used to reduce lifetime measurements for the resonance and intercombination lines to quantities proportional to the square of their radial transition matrix elements. If we denote these quantities as "reduced line strength factors" $S_{\rm r}$, they are given by

$$S_{\rm r}({\rm Res}) \equiv S({\rm Res})/\cos^2\theta\,, \tag{27.8}$$

$$S_{\rm r}({\rm Int}) \equiv S({\rm Int})/\sin^2\theta\,. \tag{27.9}$$

As illustrated for the $5s^2$–5s5p transitions in the Cd sequence in the lower panel of Fig. 27.10, these scaled reduced line strength factors (like the alkali-metal-like case) exhibit a linearity vs. reciprocal screened charge that converges to the hydrogenic value at infinite Z.

This formulation permits another type of test of relativistic corrections. In the nonrelativistic limit, the Schrödinger equation and LS coupling should be expected to hold, and govern the IC amplitudes. However, for highly complex atoms, the use of the Dirac equation and jj coupling becomes necessary. In that limit, the spin dependence occurs not only in the angular-momentum portion of the wave function, but also in its radial portion. In the Dirac equation, there are two radial wave functions, corresponding to $(j, j') = (\frac{1}{2}, \frac{1}{2})$ and $(\frac{1}{2}, \frac{3}{2})$.

Interestingly, the reformulation relative to the jj limit yields a mixing angle that is very similar to that of the nonrelativistic case, but with a phase shift ξ dictated by the difference between the radial matrix elements. If we denote the radial transition integrals as $R_{2j,2j'}$, the relativistic analogue of (27.8) and (27.9) has been shown to be

$$S_r({\rm Res}) \equiv S({\rm Res})/\cos^2(\theta - \xi)\ , \tag{27.10}$$

$$S_r({\rm Int}) \equiv S({\rm Int})/\sin^2(\theta - \xi)\ , \tag{27.11}$$

where

$$\tan\xi \equiv \sqrt{2}(R_{31} - R_{11})/(2R_{31} + R_{11})\ . \tag{27.12}$$

MCDF calculations for these quantities have been made that indicate that these effects are negligible for all but the Hg isoelectronic sequence. The correction is most significant for the lower ions of the sequence, where the angular portion of the mixing is smallest. A plot of the mixing-angle linearization, with and without this correction, is shown in the upper panel of Fig. 27.11. The effect on the exposition of the line strength factors is shown in the lower panel of Fig. 27.11. Prior to this correction, the points for the first two charge states for the intercombination transitions dipped below the trend at higher Z. The application of this correction moved the Hg I and Tl II points onto the linear trend. Note that for this sequence only four stable ions exist, but the trend permits accurate predictions for the radioactive members of the sequence.

A similar analysis can be applied to the $2p^6$–$2p^5 3s$ transitions in the Ne isoelectronic sequence. Here the fact that the transitions have $\Delta n = 1$ rather than $\Delta n = 0$ results in much shorter lifetimes (because of the wavelength-cubed dependence). For highly charged ions these lifetimes are too short to be measured by time-of-flight and too long to be measured by line widths, but they have important applications in, for example, X-ray laser technology. Thus the accurate extrapolation of the measurements accessible to BFS measurement is valuable.

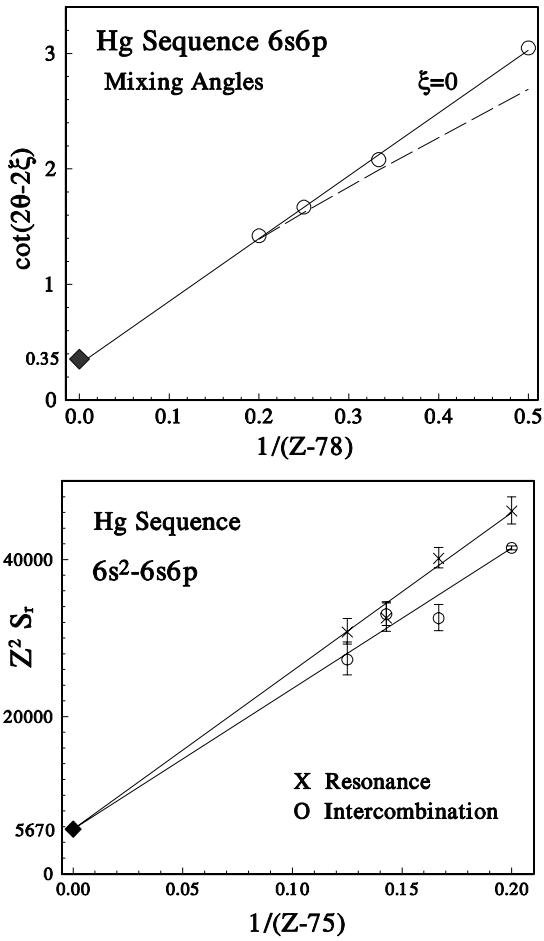

Fig. 27.11. Mixing angles and scaled reduced line strength factors for the Hg isoelectronic sequence

27.5.3 High-n and -ℓ States

When a multiply charged fast ion beam is sent through a thin foil it can capture an electron at the foil exit, producing a state of very high n and ℓ. Such states are also formed in many other types of light sources. In thermonuclear fusion plasmas, such states are populated by charge exchange, between multiply charged ions in the plasma and fast beams of neutral H and He injected into the plasma for auxiliary heating. Accurate wavelengths are crucial for the determination of the plasma temperature. However, when formed in denser plasmas, these states tend to be destroyed by Stark quenching (electric-field mixing of the individual ℓ states) or collisional deexcitation. Because of the tenuous nature of the beam–foil plasma, these states persist there until they

decay radiatively, and thus can provide much valuable information about the ion.

The circular-orbit ($\ell = n - 1$) transitions in the so-called "yrast" chain are unbranched, and produce strong features in beam–foil spectra, as do the adjacent "yrare" ($\ell = n - 2$, $\ell = n - 3$) transitions. For sufficiently high n these states are nonpenetrating, and the inner electrons can be treated as a deformable core of charge that can be characterized by effective dipole and quadrupole polarizabilities $\alpha_{\rm d}$ and $\alpha_{\rm Q}$, and a nonadiabatic correlation parameter β. This formulation is known as the "core polarization model", wherein the term value T of a level n, ℓ can be written as

$$T = T_{\rm H} + \alpha_{\rm d}\langle r^{-4}\rangle + (\alpha_{\rm Q} - 6\beta)\langle r^{-6}\rangle \ . \tag{27.13}$$

Here $T_{\rm H}$ is the value for a corresponding hydrogenlike (single-electron) ion with a nuclear charge equal to the net charge of the ion (the nucleus dressed in the electronic core), and $\langle r^{-k}\rangle$ is the expectation value for the radius raised to the power k in this hydrogenlike ion. Wavelength measurements for a sampling of yrast and yrare transitions in a given system permit the determination of the two parameters $A = \alpha_{\rm d}$ and $B = \alpha_{\rm Q} - 6\beta$ for its ionic core.

These quantities not only permit the prediction of all other levels and transitions of high n and ℓ in the system, but also provide electric polarizabilities that describe the ionic core in the presence of any external electric field. These nonpenetrating orbitals provide a gentle probe of the inner core, and differences in the interaction energies between orbitals that differ slightly in n and ℓ values can reveal subtle properties of the ionic core.

27.5.4 Multiply Excited States

Because of the high collisional density within the solid foil and the opportunity for electron pickup by the beam particles at the downstream surface of the foil, the beam–foil source produces a copious population of states with multiple electron excitation, core vacancies, and core excitation. Doubly excited states are also populated in laboratory and astrophysical plasmas by the process of dielectronic recombination, i.e. the capture of a free electron and simultaneous excitation of a bound electron. Such states have a different ionization limit from that of the singly excited states, and autoionization (radiationless electron ejection) often leads to very short characteristic lifetimes for these states. There are situations, however, in which autoionization channels are either forbidden or inhibited, and radiative decay is observable.

For example, the quartet levels of the $1s2s n\ell$ and $1s2p n\ell$ ^{4}L systems in the Li isoelectronic sequence are normally not able to autoionize into the $1s^2\epsilon\ell$ doublet continuum by the Coulomb interaction (because of the $\Delta S = 0$ selection rule), but they can decay to lower quartet states by E1 radiative transitions. However, spin-forbidden E1 transitions to the $1s^2 n\ell$ ^{2}L doublet

system, as well as spin–orbit-induced autoionization, are sometimes possible. An interesting case involves the $1s2p^2\ {}^4P_J$ levels, in which a weak mixing of the $1s2p^2\ {}^4P_{5/2}$ level with the rapidly autoionizing $1s2p^2\ {}^2D_{5/2}$ level causes its lifetime to be substantially shortened relative to that of the other ${}^4P_J$ fine-structure levels. This "differential metastability" is similar to that encountered in Sect. 27.4.2 for the Be-like $2s3p\ {}^3P_J$ levels, except that here the added decay channel is to the continuum rather than to the ground state.

27.5.5 QED Corrections

The Lamb shift S traditionally refers to the energy difference between the $2s\ {}^2S_{1/2}$ and $2p\ {}^2P_{1/2}$ levels in hydrogen, caused by quantum electrodynamic (QED) effects. It is particularly interesting to study S along an isoelectronic sequence. It took nearly 20 years before it could be experimentally determined for the doubly ionized system Li^{2+}, using an electrostatic accelerator. Nowadays experimental data exist for many systems, including hydrogenlike U^{91+}.

Lamb shift studies have also been extended to He-like atoms. For instance, the wavelengths of the $1s2s\ {}^3S$–$1s2p\ {}^3P$ transitions have been accurately measured for many systems, from He to Xe^{52+}. The agreement between theory and experiment is excellent.

27.5.6 Hyperfine Quenching

An interesting aspect of the theory of highly forbidden transitions is the effect of hyperfine quenching, whereby mixing induced by interactions with the magnetic moment of the nucleus can significantly alter the lifetimes of the levels.

An illustration involving the lifetimes of the $1s2p\ {}^3P_J$ levels in the helium isoelectronic sequence is shown in Fig. 27.12. With increasing Z, variously forbidden transitions to the $1s^2\ {}^1S_0$ ground state have an increasingly important effect on the lifetimes of the individual fine-structure levels. At low Z all three levels have similar lifetimes, since the E1 transition to $1s2s\ {}^3S_1$ dominates. With increasing Z the lifetime of the ${}^3P_1$ level is drastically shortened, since the $\Delta S \neq 0$ selection rule is valid only for pure relativistic LS coupling, and spin mixing opens the relativistic-E1 transition to ground. A similar but less drastic shortening of the ${}^3P_2$ lifetime occurs because of its M2 transition to ground. For systems with nonzero nuclear spin I, both the ${}^3P_2$ and the ${}^3P_0$ lifetimes are affected by hyperfine-induced E1 transitions to the ground state. This is particularly striking for the ${}^3P_0$ level, because for a spinless nucleus it would have *no* radiative decay channel to ground, and because for $J = 0$ the effect is not smeared over a multiplicity of values for $F = I + J$.

As can be seen from Fig. 27.12, there is a sharp turning on of the hyperfine quenching effect at $Z = 21$, and the alternating zero and nonzero I

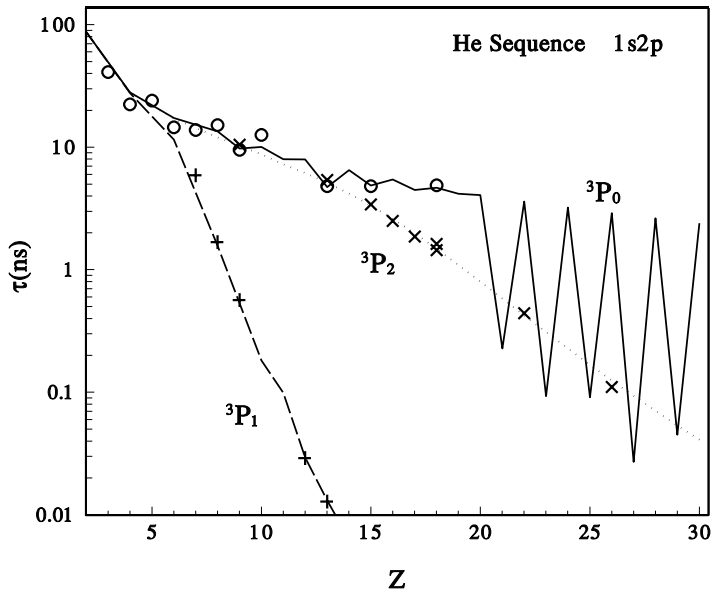

Fig. 27.12. Hyperfine quenching in the He isoelectronic sequence

values in the most abundant isotopes of nuclei of even and odd Z produce a sawtooth pattern in the lifetimes. This plot describes measurements involving only the most abundant isotope, but isotopically enriched samples are available at some accelerator facilities. Thus these studies have been extended to obtain precision measurements of the hyperfine quenching by differential comparisons of lifetimes for systems with the same Z but with isotopes of both even and odd A.

27.6 Future Challenges

While much progress has been made through the application of accelerator-based studies of atomic structure, significant problems remain that must be addressed to achieve fundamental understanding and the application-enabling goals of the field. Many examples exist, and we mention here only a sampling.

27.6.1 Calibration Standards

While great strides have been made in the precision and scope of atomic-lifetime measurements, little work has been done on the specification of branched transition probabilities in multiply charged ions. In order to convert lifetime data for levels with multiple exit channels into transition probabilities, branching fractions are needed. These require the measurement of

relative intensities of the various transitions from a given upper level. For multiply charged ions, virtually no branching-ratio measurements exist. This lack of measured data leads to a corresponding lack of tests of theoretical methods for the computation of transition probabilities in complex ions.

Progress has been made in the determination of branching fractions in neutral and singly ionized atoms through the use of absolute emission, absorption, and dispersion measurements, and through combined measurements of relative branching ratios and lifetimes. However, even this work has been restricted to the visible spectrum because of the limited availability of intensity calibration standards. No comprehensive set of calibration standards is currently available for the ultraviolet region.

The reasons for the dearth of branching-fraction data in multiply charged ions are clear. Their measurement requires an intensity calibration of the detection apparatus as a function of wavelength, which is particularly difficult for multiply charged ions and for wavelengths for which reflective and refractive optics cannot be used. Moreover, it is not sufficient to obtain branching-ratio data. Complete branching fractions which include all exit channels open to a decaying level are necessary, and these may include, in addition to the visible region, significant branching via ultraviolet and infrared transitions. While BFS methods provide a powerful means of producing highly ionized atoms, they involve Doppler broadenings and shifts, polarizations due to anisotropic excitation, time variations due to decay and repopulation, etc. Thus, the use of a lab-fixed standard lamp is not optimal for intensity-vs.-wavelength calibration of a detection system that views a moving beam. A two-step process would be preferable, using a standard lamp to calibrate relative branching ratios in a suitably chosen ion, and then using that ion as an in-beam calibration standard that can be accelerated to a velocity matching that of the desired ion.

The lack of transition probability data is particularly troublesome for the study of isoelectronic sequences. Expositions of line strength data often exhibit slowly varying, nearly linear isoelectronic variations. This is because wavelength and intermediate-coupling factors present in the transition probabilities are removed when converted to effective line strength factors, which have a simple dependence on the nuclear charge Z. In contrast, the reciprocal lifetime for a branched transition is summed over decay channels with different wavelength factors, resulting in a complicated dependence on Z.

Fortunately, isoelectronic measurements and semiempirical parametrizations can be employed to obtain calibration standards. A promising example involves systems with ground configurations ns^2np^2 such as the Si, Ge, Sn, and Pb isoelectronic sequences. The ground term can be specified by two mixing angles (entangling $^3P_2$ with $^1D_2$ and $^3P_0$ with $^1S_0$), and the $ns^2npn's$ excited term can be specified in terms of a third mixing angle (entangling $^3P^o_1$ with $^1P^o_1$). If these are nearly pure configurations (with little CI), the relative transition rates are specified by these three mixing angles. This has been

tested for transitions in the neutral atoms of these sequences, for which precision measurements of the branching fractions exist, and the semiempirical calculations show striking agreement with the measured branching fractions. Moreover, tests utilizing the empirical overdetermination of the mixing angles confirm that CI effects are negligible. Ultraviolet standards can be obtained by isoelectronically extending these formulations to the multiply charged ions.

27.6.2 Coincidence Methods

Coincidence techniques provide a powerful means for measuring lifetimes. However, such methods were difficult to apply to BFS earlier because of the low detection efficiencies in the optical wavelength region, which made accidental coincidences a serious problem. As the acceleration energy (and hence the degree of ionization) is increased, the photon energies become sufficiently large to permit the use of detectors such as those designed for nuclear-physics applications.

An application of coincidence techniques to the decay of the metastable $1s2s\ ^1S_0$ level in He-like bromine is given in Fig. 27.13. Single-E1-photon decay of this level is absolutely forbidden because both the upper and the lower ($1s^2\ ^1S_0$) level have $J = 0$, so the decay occurs by the emission of either a single M1 photon or two E1 photons. Through the use of Si(Li) detectors it is possible not only to gate the coincidence, but also to measure the energies of the photons detected.

Figure 27.13 shows a plot of the intensity of the coincidence events plotted as a function of the energies of the individual photons. The diagonal line represents coincidences between the two simultaneously emitted E1 photons, which sum to the total excitation energy of 12 keV. The peak that occurs when both photons have 12 keV represents accidental coincidences between two unrelated M1 photons. The two rows that occur at a single photon energy of 12 keV represent accidental coincidences between one M1 and one continuum photon. Such applications of coincidence techniques offer many possibilities for new types of measurements of high precision and reliability.

27.7 Conclusion

Accelerator-based atomic spectroscopy has already made significant contributions to the fundamental understanding of atomic structure and its available database, and it has the potential to provide essential new data of unprecedented accuracy and scope. This work can be carried out with existing accelerator facilities, and the diversity of accelerators available is an important part of the strength of the method.

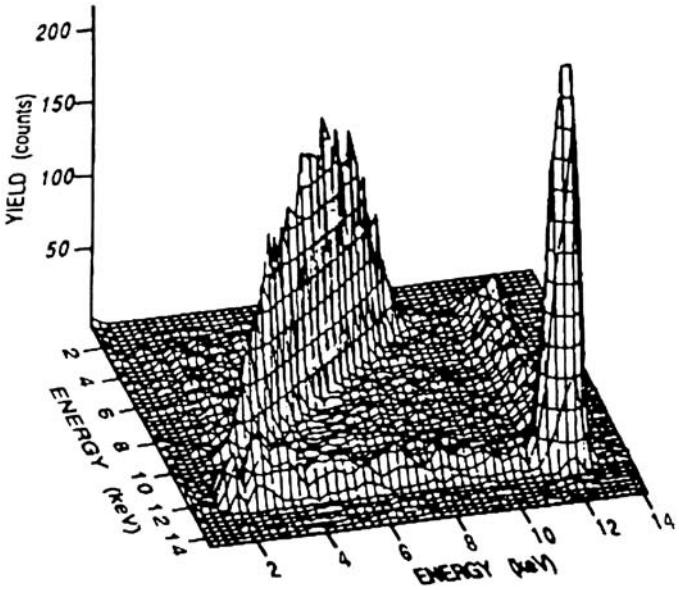

Fig. 27.13. Coincidence measurement of a two-photon decay

References

1. L. J. Curtis, *Atomic Structure and Lifetimes: a Conceptual Approach* (Cambridge University Press, Cambridge, UK 2003)
2. L. J. Curtis and I. Martinson, in *Atomic Physics with Heavy Ions*, H. F. Beyer and V. P. Shevelko, editors (Springer, Heidelberg, 1999) pp. 197–218
3. E. Träbert, in *Accelerator-Based Atomic Physics: Techniques and Applications*, S. M. Shafroth and J. C. Austin, editors (AIP Press, New York, 1998) pp. 567–600
4. E. H. Pinnington, in *Atomic, Molecular, and Optical Physics Handbook*, G. W. F. Drake, editor (AIP Press, New York, 1996) pp. 213–219